A&A 452, 75–81 (2006)
DOI: 10.1051/0004-6361:20054508

Astronomy & Astrophysics

The radial profiles of the different mass components in galaxy clusters⋆

A. Biviano[1] and P. Salucci[2]

[1] INAF/Osservatorio Astronomico di Trieste, via G. B. Tiepolo 11, 34131 Trieste, Italy
e-mail: biviano@oats.inaf.it
[2] International School for Advanced Studies SISSA/ISAS, via Beirut 2–4, 34013 Trieste, Italy
e-mail: salucci@sissa.it

Received 10 November 2005 / Accepted 19 February 2006

ABSTRACT

Aims. To derive the mass profiles of the different luminous and dark components in clusters.
Methods. The cluster mass profile is determined by using the Jeans equation applied to the projected phase-space distribution of about 3000 galaxies members of 59 nearby clusters from the ESO Nearby Abell Cluster Survey. The baryonic and subhaloes mass components are determined from the galaxies' luminosity-density profiles through scaling relations between luminosities and baryonic and dark halo masses. The baryonic mass component associated with the intra-cluster gas is determined using X-ray data from *ROSAT*.
Results. The baryon-to-total mass fraction decreases from a value of $\simeq$0.12 near the center to $\simeq$0.08 at the distance of $\simeq$0.15 virial radii, then it increases again, to reach a value of $\simeq$0.14 at the virial radius. Diffuse, cluster-scale dark matter dominates at all radii, but its contribution to the total mass content decreases outwards to the virial radius, where the dark matter in subhaloes may contribute up to $\simeq$23%, and the baryons $\simeq$14% of the total mass. The dark mass and diffuse dark mass profiles are well fit by both cuspy and cored models. The subhalo mass distribution is not fit by either model.

Key words. cosmology: observations – galaxies: clusters: general – galaxies: kinematics and dynamics – cosmology: dark matter

1. Introduction

With the increasing accuracy of cosmological numerical simulations, the study of the mass profiles of galaxies and galaxy clusters has become a powerful way to constrain cosmological models. With numerical simulations, Navarro et al. (1996, NFW hereafter) found that dark matter (DM hereafter) haloes are characterized by a universal mass-density profile, simply summarized by two power-law regimes, an inner one with exponent −1, and an outer one with exponent −3. The universality of the profile and the existence of a central cusp have been confirmed (Moore et al. 1999; Diemand et al. 2004; Navarro et al. 2004; but see Ricotti 2003).

It is obvious that observational knowledge of the mass profiles of the dark and baryonic matter in clusters provides crucial insights into their formation and evolution (see, e.g., Gao et al. 2004; Springel et al. 2001). In particular, one aspect of the ΛCDM theory that can be tested is the presence of a cusp in the center of the DM halo. It is well known that on galactic scales mass profiles of the NFW form are unable to account for the rotation curves of low-surface brightness galaxies (de Blok & Bosma 2002), normal spirals (de Blok et al. 2003; Gentile et al. 2004), and the fundamental plane of ellipticals (Borriello et al. 2003).

On cluster scales, the situation is far more open. Cluster mass profiles have been obtained from the analyses of the X-ray emitting intra-cluster (IC hereafter) gas, of the projected phase-space distribution of cluster galaxies, and of the gravitational lensing shear pattern of background galaxies. Most results indicate consistency with the NFW profile (see, e.g., Allen et al. 2000; Athreya et al. 2002; Biviano & Girardi 2003; Jee et al. 2005; Katgert et al. 2004, hereafter KBM; Łokas et al. 2006; Pratt & Arnaud 2005; Rines et al. 2003; Rines & Diaferio 2006). In some cases a flatter than NFW profile is preferred (Broadhurst et al. 2005; Ettori et al. 2002; Kelson et al. 2002; Nevalainen et al. 2000), or even required (Arieli & Rephaeli 2003; Demarco et al. 2003; Sand et al. 2004). While isothermal profiles were rejected by some dynamical analyses (e.g. Rines et al. 2003; Broadhurst et al. 2005), cored profiles generally were not excluded (see however Dahle et al. 2003), as far as the core of the matter distribution is small (Arieli & Rephaeli 2003; Biviano & Girardi 2003; KBM).

In order to allow a proper comparison of the results of simulations with observations, it is important to determine the *total* mass distribution and its major components, baryons and the subhaloes. In particular, the baryonic contribution has been shown to be relevant in clusters, both near the centre because of the substantial contribution from the cD (e.g. Sand et al. 2004), and in the outer regions, because of the increasing mass fraction of the IC gas (e.g. Łokas & Mamon 2003). Recently, KBM have derived a synthetic mass profile of rich galaxy clusters, using the ESO Nearby Abell Cluster Survey (ENACS) data-set (Katgert et al. 1998). KBM found that the total cluster mass profile is well fitted both by a NFW profile, and by a Burkert (1995) profile. KBM also found that the total mass profile is very well traced by the luminosity profile of the early-type galaxies, i.e. the mass-to-light ratio is almost flat, when only early-type galaxies are selected, and the brightest members are excluded. The aim of this paper is to derive the mass distribution of the DM, of the baryonic matter and of the cluster sub-haloes, separately. We use the same data-set of KBM analysed in a slightly different way (see Sect. 2.1). We use the X-ray data from

⋆ Based on observations collected at the European Southern Observatory (La Silla, Chile).

Reiprich & Böhringer (2002) to determine the radial profiles of the IC gas, and the luminosity-density profiles of cluster galaxies to determine the mass distributions of the galaxy baryons and of the DM subhaloes.

The structure of this paper is as follows: in Sect. 2 we determine the mass profiles of the different cluster components; in Sect. 3 we fit models to the observed mass profiles; in Sect. 4 we summarize our results and draw our conclusions. Throughout this paper we adopt $H_0 = 70$ km s^{-1} Mpc^{-1}, $\Omega_m = 0.3$ and $\Omega_\Lambda = 0.7$.

2. Mass profiles

2.1. Total mass

We use the data-set of 59 clusters used by KBM and described in Biviano et al. (2002). These clusters are combined into a single "ensemble" cluster, in order to improve the rather poor number statistics of individual clusters. This gives a total sample of ∼2900 member galaxies with positions and redshifts. Note that Sanchis et al. (2004) have shown that a stacked sample of several galaxy clusters can be used to determine a reliable average mass profile of individual clusters.

The stacking is done in the space of normalized clustercentric distances, R/r_{100}, and normalized velocities with respect to the cluster mean velocity, $(v - \overline{v})/\sigma_v$, where r_{100} is the radius of the sphere around the cluster centre with mean density equal to 100 times the critical density, and σ_v is the global velocity dispersion. For the scaling of clustercentric distances, Biviano et al. (2002) used Carlberg et al.'s (1997) proxy for r_{200} (the radius of the sphere around the cluster centre with mean density equal to 200 times the critical density), which is based on the assumption of an isothermal mass profile. However, the cluster mass profile determined by KBM is not isothermal, therefore, for the estimation of both r_{100} and r_{200} (needed for the determination of the IC gas mass profile, see Sect. 2.2), we prefer to use Popesso et al.'s (2005) relation (see Eq. (1) in that paper) which makes explicit use of the shape of the mass density profile determined by KBM. The average values of σ_v and r_{100} for our cluster sample are 699 km s^{-1} and 2.25 Mpc, respectively, and the average virial mass is $M(<r_{100}) = 6.5 \times 10^{14}\, M_\odot$.

To determine the mass profile of the ensemble cluster ($M_{tot}(r)$ in the following), we first apply the isotropic Jeans equation on the early-type cluster members, as described in KBM. The errors on $M_{tot}(r)$ are obtained from 64 bootstrap resamplings of the data (see KBM for more details). Near-isotropy for the early-type cluster members was inferred by KBM from the analysis of the whole velocity distribution of these galaxies. Support for the isotropic assumption also comes from the analysis of Biviano & Katgert (2004) of the orbits of different cluster galaxy populations. Here we go beyond KBM's isotropic assumption, and we also consider solutions with constant orbital anisotropy $\mathcal{A} \neq 0$, where $\mathcal{A} \equiv 1 - \langle v_t^2\rangle/\langle v_r^2\rangle$, and $\langle v_r^2\rangle$, $\langle v_t^2\rangle$ are the mean squared components of the radial and tangential velocity, respectively (see, e.g., Binney & Tremaine 1987). Since KBM constrained the velocity anisotropy of the early-type galaxy population to lie in the range $-0.6 \lesssim \mathcal{A} \lesssim 0.1$, we determine $M_{tot}(r)$ for the two extreme cases $\mathcal{A} = -0.6$ and $\mathcal{A} = 0.1$, using the anisotropic Abel inversion (Mamon & Boué 2006) and Jeans equations. The results are shown in Fig. 1, where we display the circular velocity profiles, $V_c \equiv (GM_{tot}/r)^{0.5}$. While the isotropic solution for the total mass profile is not significantly different from that derived by KBM, orbital anisotropy has some effect on the uncertainty of the total mass profile.

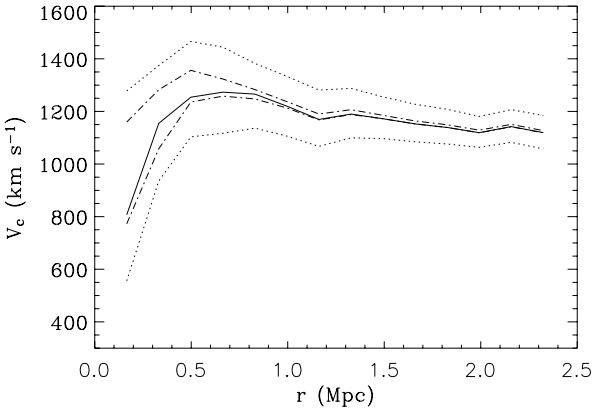

Fig. 1. The circular velocity profiles, $V_c \equiv (GM_{tot}/r)^{0.5}$, of the total mass, obtained assuming isotropy ($\mathcal{A} = 0$, solid line), mild radial anisotropy ($\mathcal{A} = 0.1$, lower dash-dotted line), and mild tangential anisotropy ($\mathcal{A} = -0.6$, upper dash-dotted line). The dotted lines delimit the ± 1-σ intervals accounting for both the random errors (as obtained from 64 bootstrap resamplings of the data in the isotropic case), and systematic errors (arising from the uncertainty on the value of the velocity anisotropy $\mathcal{A}$).

2.2. Baryonic mass: IC gas

To determine the mass profile of the IC gas ($M_{gas}(r)$ in the following), we use the IC gas density profiles. Unfortunately these are available only for a subset of our 59 cluster sample. This subset is characterized by a larger average velocity dispersion than the whole sample. Since the shape of the IC gas density profile depends on the cluster X-ray temperature (Mohr et al. 1999), and hence also on the cluster velocity dispersion, we cannot use the subset of clusters with available X-ray data as representative of the whole sample.

We proceed instead as follows. We consider Reiprich & Böhringer's (2002) sample of clusters for which the best-fit parameters of the β-profiles (Cavaliere & Fusco-Femiano 1978) are available,

$$\rho_{IC} = \rho_0 \left[1 + (r/r_c)^2\right]^{-(3/2)\beta}. \quad (1)$$

We then consider the distribution of velocity dispersions of our 59 clusters, and convert it into a distribution of pseudo X-ray temperatures, using the empirical relation of Girardi et al. (1996). We generate 500 bootstrap sets of this pseudo-T_X distribution. For each of these bootstrap sets, we then extract 59 clusters from the sample of Reiprich & Böhringer (2002), chosen to have a T_X-distribution as close as possible to the pseudo-T_X distribution of the bootstrap set. We finally compute the average values of r_c and β for the 59×500 extracted clusters (many of the clusters are of course extracted more than once, as expected for a bootstrap procedure), $\langle\beta\rangle = 0.625 \pm 0.007$, and $\langle r_c\rangle = (0.0636 \pm 0.0004)\, r_{200}$. We use these values to define the average gas density profile, which is meant to be representative of our cluster sample. Integration of this average gas density profile provides the IC gas mass profile, apart from a constant, that we fix to the average gas-to-total mass fraction at r_{200} as determined by Ettori (2003) for a sample of nearby clusters, $0.11^{+0.03}_{-0.02}$.

There is an additional uncertainty that is related to the extrapolation of the observed IC gas profiles to r_{200}. Most of the IC gas profiles on which $M_{gas}(r)$ is based are determined from data at radii smaller than $\sim r_{500}$ (the radius of the sphere around the cluster centre with mean density equal to 500 times the critical density) corresponding to ∼1 Mpc in our cluster sample. In order

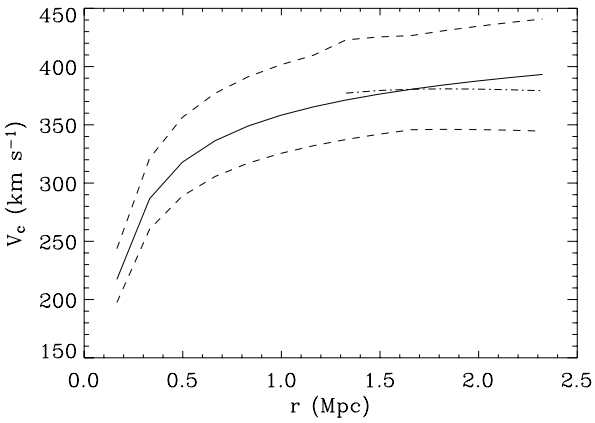

Fig. 2. The contribution of the IC gas mass to the circular velocity profile, $V_c \equiv (GM_{gas}/r)^{0.5}$ (solid line), obtained from the sample of Reiprich & Böhringer (2002). The dash-dotted line shows the effect of using Neumann's (2005) steeper IC gas density profile in the radial range $>r_{500}$. The dashed lines delimit the ± 1-σ intervals accounting for the uncertainties in the best-fit parameters of the IC gas density profile, as well as for the uncertainty in the value $(M_{gas}/M_{tot})(r_{200})$.

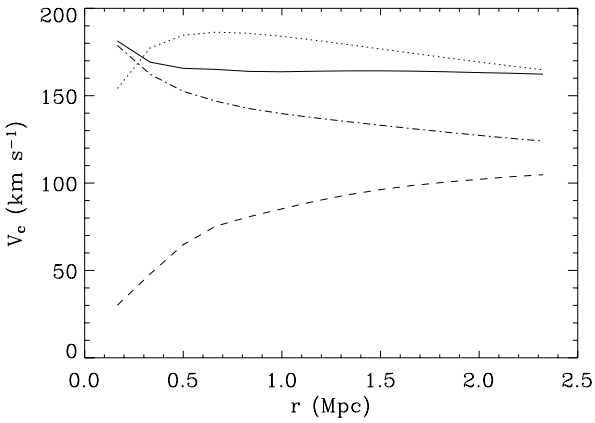

Fig. 3. The contributions to the circular velocity profile of the baryonic mass in all cluster galaxies (solid line), in early-type cluster galaxies (dash-dotted line), and in late-type galaxies (dashed line). The dotted line shows the profile derived by Łokas & Mamon (2003) for the Coma cluster, after appropriate scaling (see text).

to deal with the systematic uncertainty related to this extrapolation, we take into consideration the analysis of Neumann (2005). Neumann has analysed a sample of 14 nearby clusters, for which she has been able to trace the X-ray emission beyond r_{200}. She concluded that the IC gas density profile steepens with increasing radius. Out to 1.2 r_{200} Neumann found a best-fit β-profile[1] with $r_c = 0.19\, r_{200}$ and $\beta = 0.8$. The fitted profile is therefore significantly steeper than the mean profile we have found by using the sample of Reiprich & Böhringer (2002).

We then adopt Neumann's best-fit to estimate the uncertainty involved in the extrapolation of our average IC gas density profile to radii $>r_{500}$. We find that M_{gas} is not strongly modified beyond r_{500} (and out to $1.5\, r_{200}$), despite the substantial change in the IC density profile, since the normalisation of the gas mass profile at r_{200} is fixed, $(M_{gas}/M_{tot})(r_{200}) = 0.11^{+0.03}_{-0.02}$. Hence, the uncertainty on the resulting M_{gas} is mostly driven by the uncertainty in the normalization of the gas-to-total mass fraction at r_{200}. In Fig. 2 we show the resulting contribution of the IC gas mass component to the circular velocity profile, with its confidence interval, accounting for the uncertainties in the best-fit parameters of the IC gas density profile, and in the normalisation value $(M_{gas}/M_{tot})(r_{200})$.

2.3. Baryonic mass: galaxies

In order to determine the baryonic mass profile in the galactic component ($M^{lum}_{gal}(r)$ hereafter) we consider separately the two classes of early- and late-types (we use the data-set of Thomas & Katgert 2006, for the morphological/spectral classification of ENACS galaxies). The baryonic mass profiles of these two galaxy classes are obtained following the prescriptions of KBM for the derivation of their number density profiles (see Appendix B in KBM; see also Biviano & Katgert 2004). KBM's methodology accounts for both the incomplete azimuthal coverage of the ENACS observations (Katgert et al. 1996, 1998), and the fact that different clusters are sampled out to different fractions of their virial radii.

[1] Among the subsamples of Neumann (2005) we have chosen her No. 1, based on the similarity between the T_X distribution of this subsample and of our clusters.

In KBM the number density and the luminosity density profiles were derived; here we proceed further by assuming (for each galaxy class) a relation converting a given galaxy luminosity to its baryonic component. For the early class we take Borriello et al.'s (2003, see their Eq. (15)) relation, and convert their magnitudes to the R-band magnitudes of ENACS galaxies (Katgert et al. 1996), using the relations of Fukugita et al. (1995). For late-type galaxies the relationship between luminosities and baryonic masses is taken from Salucci & Persic (1999, see their Eqs. (3)–(5)).

Since the ENACS sample is not complete, we need to correct the density profiles for incompleteness. We estimate that the ENACS sample is roughly 75% complete down to an apparent magnitude $R = 16.5$ (see Fig. 4 in Katgert et al. 1998), and then the completeness rapidly drops for fainter magnitudes. At the median redshift of our clusters ($z = 0.064$), $R = 16.5$ corresponds to an absolute magnitude $M_R = -20.8$. For simplicity, we then assume 0.75 completeness down to $M_R = -20.8$, and zero at fainter magnitudes.

In order to derive the luminosity of galaxies fainter than $M_R = -20.8$, we use the R-band luminosity function of Lugger (1986), that is a Schechter (1976) luminosity function with $M^\star_R = -21.9$ and $\alpha = -1.24$. We integrate it between $M_R = -20.8$ and the magnitude corresponding to $0.01 L^\star_R$, where $L^\star_R$ is the luminosity corresponding to $M^\star_R$. We further assume that most faint cluster galaxies with $M_R \geq -20.8$ are dwarf spheroidals, i.e. early-type galaxies. We find that galaxies fainter than $M_R = -20.8$ contribute 25% of the galactic baryonic mass in a cluster. We then correct the observed baryonic profiles for the faint galaxies contribution, and for the additional factor $1.33 = 1/0.75$, that accounts for the overall spectroscopic incompleteness.

The resulting contribution of the baryonic mass in cluster galaxies to the circular velocity profile is shown in Fig. 3. In the same figure we also show the separate contributions of the baryonic mass in early-type and late-type galaxies. The profile of the baryonic mass in early-type galaxies is similar to that of the total mass, but more centrally concentrated. The profile of late-type galaxies is instead less centrally concentrated than the total mass profile. Early-type galaxies dominate the galactic baryonic budget within the virial radius, but the contribution of late-type galaxies to this budget increases with radius, from only 3% near the center to ∼40% within the virial radius.

In order to put our galaxy baryonic mass profile in context, we compare it with that derived by Łokas & Mamon (2003) for the Coma galaxy cluster. First we compute the ratios between the Coma virial radius and total mass and the corresponding average values for our 59 clusters (these ratios are 1.3 and 1.9, respectively). We then rescale Łokas & Mamon's profile using these scaling factors, and assuming that the cluster baryonic mass scales proportionally to the cluster total mass. The result is shown as a dashed line in Fig. 3. Clearly, Łokas & Mamon's profile is less concentrated than ours, but it does not differ by more than ±20% over the whole radial range considered here. We consider this a remarkable agreement, given the fact that Coma is not a typical galaxy cluster. While 80% of our clusters are dominated by a single brightest cluster galaxy (BCG hereafter), two BCGs are present in the inner region of Coma, which is in fact substructured (see, e.g., Adami et al. 2005, and references therein). The presence of substructures in the Coma cluster core probably reduces the concentration of its baryonic mass profile.

2.4. Dark mass: subhaloes

The distinction between DM in subhaloes and diffuse DM is to some extent a matter of definition. Here we consider as subhaloes all visible cluster galaxies (including those we miss because of the completeness limit of the ENACS survey), with the exception of the BCG. Since the BCG is centrally located, its diffuse stellar and DM haloes are generally considered part of the diffuse IC material (Lin & Mohr 2004; Murante et al. 2004).

We compute the subhalo mass profile ($M_{\rm sub}(r)$ in the following) from the average luminosity density profiles of the cluster member galaxies, by adopting a Hubble-type dependent scaling relation between a galaxy luminosity and its halo mass (see Shankar et al. 2006). As in Sect. 2.3, we apply the needed corrections for incompleteness. Galaxies fainter than the spectroscopy limit of the ENACS survey ($M_R \simeq -20.8$) contribute roughly 30% of the subhaloes mass. An additional factor of 1.33 must be included to account for the average incompleteness of the ENACS spectroscopic sample (see Sect. 2.3).

The resulting subhalo mass profile needs however to be modified to take into account the fact that, unlike in the field, galaxies in clusters are so densely packed that their haloes would overlap. This overlap does not in fact occur because their haloes are tidally stripped as they pass through dense regions. Numerical simulations predict a flattening of the density profiles of subhaloes near the cluster centre, and as much as a 50% loss of the total mass in subhaloes, due to the stripping process (see, e.g., Gao et al. 2004). Gravitational lensing observations confirm that the haloes of galaxies near the cluster centres are indeed less massive than those of field galaxies (Natarajan et al. 2002; Gavazzi et al. 2004).

In order to take into account the effects of tidal stripping near the cluster centre, and given the current, rather loose, observational constraints on this topic, we try the following simplified approach. We modify our estimate of the subhalo mass as follows. First, we assume that subhalo stripping only occurs within a critical radius $R_{\rm BCG}$, and that stripping is more effective as the clustercentric radius decreases. In practice, we assume $M_{\rm sub} \approx 0$ at the cluster centre, and smoothly interpolate to the unstripped $M_{\rm sub}$ at the radius $R_{\rm BCG}$.

We consider it reasonable to identify the value of $R_{\rm BCG}$ with the radius of the halo of the BCG. BCGs can be followed photometrically out to ∼0.4 Mpc (see, e.g., Gonzalez et al. 2005). The haloes of BCGs have been modelled with a Burkert profile with scale radius $r_{\rm s} = (2.6 \pm 0.2) R_{\rm e}$ (Borriello et al. 2003), where $R_{\rm e} = 18 \pm 2$ kpc (Nelson et al. 2002), implying that 1/2 of the total BCG mass is contained in a sphere of ∼0.5 Mpc radius. Moreover, numerical simulations predict that the density profile of subhaloes deviates from the overall density profile of DM inward of $\sim 0.4\, r_{200} \simeq 0.7$ Mpc (see Fig. 1 in Gao et al. 2004). Therefore we take $R_{\rm BCG} \sim 0.5 \pm 0.2$ Mpc. The uncertainty in the value of $R_{\rm BCG}$ increases the error of $M_{\rm sub}$ in the central region.

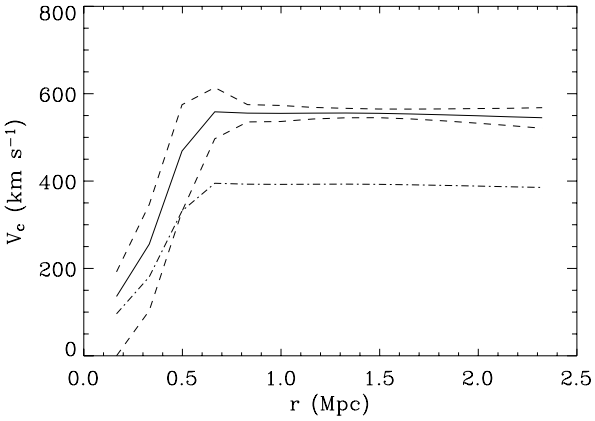

Fig. 4. The contribution of the mass in subhaloes to the circular velocity profile, $V_{\rm c} \equiv (GM_{\rm sub}/r)^{0.5}$ (solid line) and its 1-σ confidence interval (dashed lines) accounting for both the random and the systematic errors (the latter being related to the uncertainty in the size of the central stripping region). The dash-dotted line corresponds to the scenario in which subhaloes lose 50% of their total mass.

The resulting contribution of $M_{\rm sub}$ to the circular velocity profile is shown in Fig. 4. We also display the circular velocity profile corresponding to the rather extreme scenario in which 50% of the total subhaloes mass is lost at any radii (*strong stripping* scenario hereafter).

2.5. Dark mass: diffuse

The diffuse DM profile is obtained from the total mass profile by subtracting from it the baryonic mass profile, $M_{\rm dark}(r) \equiv M_{\rm tot}(r) - M^{\rm lum}_{\rm gal}(r) - M_{\rm gas}(r)$.

Baryons are a minor though not irrelevant component of the total cluster mass. On the other hand, a non-negligible fraction of the total cluster mass is in subhaloes. When both the baryonic and subhalo masses are subtracted from the total mass, we obtain what we call the diffuse DM profile $M^{\rm diff}_{\rm dark}(r) \equiv M_{\rm tot}(r) - M^{\rm lum}_{\rm gal}(r) - M_{\rm gas}(r) - M_{\rm sub}(r)$.

2.6. Relative fractions

The mass fractions of the different cluster components relative to the total cluster mass are shown in Fig. 5 as *cumulative* mass fractions within the radii on the x-axis. For clarity, confidence intervals are not shown. We only show the error-bars at r_{200}. Error intervals at other characteristic radii are listed in Table 1 (see also Figs. 1−4). The largest uncertainty is on $M_{\rm tot}$, and this affects $M^{\rm diff}_{\rm dark}$ (see also Fig. 6).

Among the baryonic components, the IC gas is clearly dominant at all radii. However, very near the cluster center, galaxies contribute almost as much baryonic mass as the gas. This is due to the presence of the cD and/or very bright galaxies near the cluster center (the phenomenon also known as "luminosity segregation", see, e.g., Biviano et al. 1992, 2002). Baryons in galaxies and the IC gas are more, respectively less, centrally

Table 1. Relative contributions of the different cluster mass components at four characteristic radii. Values in brackets are for the strong stripping scenario.

Mass component	Fraction of total mass within $0.1\,r_{100}$	r_{500}	r_{200}	r_{100}
$M_{\rm gas}$	0.07 ± 0.03	0.09 ± 0.03	0.11 ± 0.03	0.12 ± 0.03
$M_{\rm gal}^{\rm lum}$	0.04 ± 0.01	0.019 ± 0.003	0.020 ± 0.002	0.021 ± 0.002
$M_{\rm sub}$	0.04(0.02) ± 0.04	0.22(0.11) ± 0.04	0.23(0.12) ± 0.03	0.23(0.12) ± 0.03
$M_{\rm dark}^{\rm diff}$	0.85(0.86) ± 0.41	0.67(0.78) ± 0.20	0.64(0.75) ± 0.14	0.63(0.74) ± 0.13

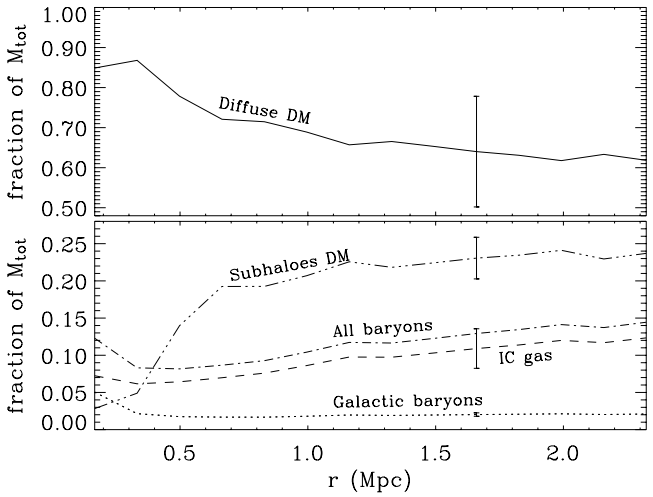

Fig. 5. The ratios between the mass profiles of the different cluster components and the total mass profile, within a given radius. Solid line: $(M_{\rm dark}^{\rm diff}/M_{\rm tot})(r)$; dotted line: $(M_{\rm gal}^{\rm lum}/M_{\rm tot})(r)$; dashed line: $(M_{\rm gas}/M_{\rm tot})(r)$; dot-dashed line: $[(M_{\rm gal}^{\rm lum} + M_{\rm gas})/M_{\rm tot}](r)$; triple dot-dashed line: $(M_{\rm sub}/M_{\rm tot})(r)$. The vertical lines indicate ±1-σ error bars at the r_{200} radius. The error bar on $(M_{\rm gal}^{\rm lum}/M_{\rm tot})(r)$ is very small and not visible in this plot. The error bar on $[(M_{\rm gal}^{\rm lum}+M_{\rm gas})/M_{\rm tot}](r)$ is not shown, since it is almost identical to the error bar on $(M_{\rm gas}/M_{\rm tot})(r)$.

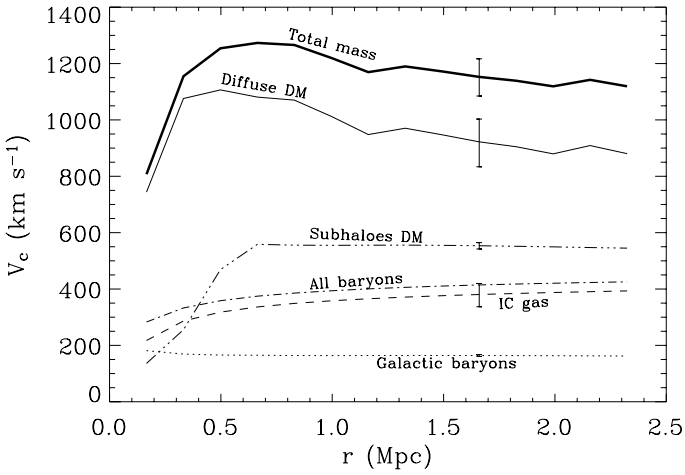

Fig. 6. The contributions of the different cluster mass components to the circular velocity profile, $V_{\rm c} \equiv (GM/r)^{0.5}$. *Upper* (thick) solid line: $M_{\rm tot}$; *lower* (thin) solid line: $M_{\rm dark}^{\rm diff}$; dotted line: $M_{\rm gal}^{\rm lum}$; dashed line: $M_{\rm gas}$; dot-dashed line: $M_{\rm gal}^{\rm lum} + M_{\rm gas}$; triple dot-dashed line: $M_{\rm sub}$. For clarity, only representative 1-σ error bars (at the r_{200} radius) are displayed. Note that the error bar on the galaxies' baryonic profile is very small and not visible in this plot. The error bar on the total baryonic profile is not shown, since it is almost identical to the error on the IC gas baryonic profile.

concentrated than the total mass; hence, the ratio of the total baryonic mass to the total cluster mass has a minimum at $\sim 0.15\,r_{100} \simeq 0.3$–$0.4$ Mpc. The ratio between the baryonic and total mass profiles is constant to within ±30% out to the cluster virial radius.

The mass contribution from the subhaloes is small near the center, where stripping may occur (see Sect. 2.4), and then increases out to 1.1 Mpc, when it reaches an approximately constant fraction of ∼0.2–0.25.

Diffuse DM is the dominant mass component at all radii. Its contribution to the total mass almost monotonically decreases with radius, except perhaps at the center, where the galactic baryons contribute significantly.

The relative contributions of diffuse and subhaloes DM change if one considers the strong stripping scenario. In this scenario, the contribution of subhaloes to the total mass budget is similar to that of all baryons (see the values listed in brackets in Table 1) and diffuse DM contributes 3/4 of the total mass.

3. Model fits

We fit the observed DM profiles with two models, the NFW and Burkert profiles. Both models are characterized by the same asymptotic slope at large radii, $\rho(r) \propto r^{-3}$, but the former is characterized by an inner cusp, the latter by a core. By comparing the results of the two model fits we can address the debated issue of the reality of the inner cusp that numerical simulations predict to exist in DM haloes.

The NFW mass density profile model can be written as:

$$\rho_{\rm NFW} = \frac{\rho_0}{(r/r_{\rm s})(1 + r/r_{\rm s})^2} \qquad (2)$$

and the Burkert profile as:

$$\rho_{\rm Burkert} = \frac{\rho_0}{(1 + r/r_0)\,[1 + (r/r_0)^2]}. \qquad (3)$$

They are both characterized by a scale radius, $r_{\rm s}$ or r_0, which, in the case of the NFW profile is usually referred to as the inverse of the concentration parameter, $c \equiv r_{100}/r_{\rm s}$, and, in the case of the Burkert profile, corresponds to the radius at which the central density drops by a factor 4.

In order to determine the best fit parameters of the two profiles, we fit the observed circular velocity profiles, $V_{\rm c}$. These are displayed in Fig. 6 for the different mass components. In order to determine the quality of the fit, we make use of the standard χ^2 analysis, applied on the mass density profiles, $\rho(r)$, instead of

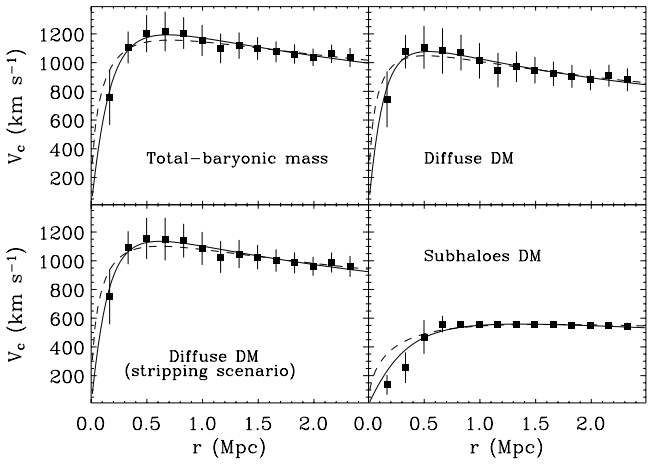

Fig. 7. *Top-left panel*: the circular velocity profile, $V_c \equiv (GM_{dark}/r)^{0.5}$, corresponding to the cluster DM profile (filled squares with 1-σ error bars), and the best-fitting Burkert (solid line) and NFW (dashed line) profiles. *Top-right panel*: same as top-left panel, for the circular velocity profile corresponding to M^{diff}_{dark}. *Bottom-left panel*: same as top-left panel, for the circular velocity profile corresponding to the cluster diffuse DM profile, assuming tidal stripping of 50% of the subhaloes mass. *Bottom-right panel*: same as top-left panel, for the circular velocity profile corresponding to M_{sub}.

on the circular velocity profiles, $V_c(r)$, since the error bars of $\rho(r)$ at different radii are independent of one another,

We start by considering the circular velocity profile corresponding to $M_{dark}(r)$. The best-fit NFW and Burkert profiles are displayed in Fig. 7, top-left panel. The results are given in Table 2, where the characteristic radii are all given in units of r_{100} ($\simeq$2.25 Mpc). Both the NFW and Burkert models provide acceptable fits to the circular velocity profile corresponding to $M_{dark}(r)$. The best-fit NFW profile has a a concentration parameter $c = 7 \pm 1$, which is in line with the predictions of cosmological simulations ($c = 8.3$ for clusters of $M(<r_{100}) = 6.5 \times 10^{14}\,M_\odot$, see Dolag et al. 2004[2]).

To fit the circular velocity profile corresponding to the diffuse DM component, both the NFW and the Burkert mass distributions become more concentrated (see Fig. 7, top-right panel, and Table 2). This is because the subtracted subhalo mass distribution is less concentrated than the total DM distribution. The best-fit r_0 value of the Burkert profile is small, but still significantly different from zero. The best-fit NFW profile has a concentration $c = 10^{+4}_{-2}$. The value of concentration does not change significantly, if we consider the strong stripping scenario ($c = 8 \pm 2$, see Fig. 7, bottom-left panel, and values in brackets in Table 2).

Neither the NFW nor the Burkert model provides acceptable fits to the circular velocity profile corresponding to $M_{sub}(r)$ (see Fig. 7, bottom-right panel, and Table 2). The rather large best-fit values of r_s and r_0 (for the NFW and Burkert model, respectively) reflect the fact that subhaloes tend to avoid the central cluster region (this was already quite clear from Fig. 5).

4. Summary and conclusions

We have obtained the mass profiles of the different cluster components, namely the baryons (in galaxies and the IC gas), the subhaloes (galactic halo DM), and the diffuse DM, out to the cluster virial radius, $r_{100} \simeq 2.25$ Mpc.

We have determined a total budget of the different mass components at different radii. The diffuse, cluster-scale, DM is the dominant cluster mass component at all radii. The total baryonic mass fraction, resulting from the summed contribution of the galactic and IC baryons, is 14% of the total cluster mass within the virial radius. The baryonic mass fraction first decreases, and then increases again with radius, changing by ±30% within the cluster virial radius. The galaxy baryonic component is always a small amount of the total mass, except near the cluster center, where galaxies contribute almost as much baryonic mass as the IC gas (because of the centrally located cD). Considering clusters as a cosmic laboratory, the low relative fraction of baryons in galaxies indicates how the star-formation in the Universe has been inefficient, since only $\simeq$14% of the baryonic mass content in clusters has been transformed in long lived stars.

The baryonic mass profile of early-type galaxies has a shape similar to that of the total mass profile (in agreement with e.g. van der Marel et al. 2000; KBM; Biviano & Girardi 2003; Łokas & Mamon 2003). On the other hand, the baryonic mass profile of late-type galaxies is less concentrated than the total mass profile. Most galaxy baryons in clusters are contributed by early-type galaxies. The IC gas-to-total mass fraction increases with radius as $r^{0.4}$ beyond $\sim$0.2 r_{100}, in agreement with previous findings (e.g. Allen et al. 2000; Łokas & Mamon 2003).

We estimate the subhalo mass fraction, 12−23%, which is in agreement with the value predicted by the results of cosmological numerical simulations (see, e.g. Takahashi et al. 2002; van den Bosh et al. 2005; Gill et al. 2004), and estimated observationally by Natarajan et al. (2002).

We obtain good fits to the DM and diffuse DM profiles with the NFW and Burkert models, while the subhalo mass profile cannot be fitted by these models. For the DM profile we obtain

$$M_{dark}/(10^{14}\,M_\odot) = 4.7\Big[\ln(1+r/0.33) - r/0.33(1+r/0.33)^{-1}\Big] \quad (4)$$

with r in Mpc, for the NFW fit, and

$$M_{dark}/(10^{14}\,M_\odot) = 1.6\Big\{\ln(1+r/0.21) - \arctan(r/0.21) + 0.5\ln\Big[1+(r/0.21)^2\Big]\Big\} \quad (5)$$

for the Burkert fit, for an average cluster of mass $M_{tot}(<r_{100}) = 6.5 \times 10^{14}\,M_\odot$, and $r_{100} = 2.25$ Mpc. For the diffuse DM profile we obtain

$$M^{diff}_{dark}/(10^{14}\,M_\odot) = 2.8\Big[\ln(1+r/0.24) - r/0.24(1+r/0.24)^{-1}\Big] \quad (6)$$

[2] Dolag et al.'s (2004) definition of c is different from that used here; we converted their values to make them consistent with the definition of c used in the present paper.

Table 2. Results of model fits to the observed mass profiles. Values in brackets are for the strong stripping scenario.

Mass profile	Model	r_s or r_0 (r_{100} units)	Reduced χ^2
M_{dark}	NFW	0.15 ± 0.03	0.3
	Burkert	0.09 ± 0.01	0.4
M^{diff}_{dark}	NFW	0.10(0.13) ± 0.03	0.3 (0.2)
	Burkert	0.07(0.08) ± 0.02	0.3 (0.3)
M_{sub}	NFW	0.33 ± 0.05	2.6
	Burkert	0.19 ± 0.02	2.4

for the NFW fit, and

$$M^{\rm diff}_{\rm dark}/(10^{14}\,M_\odot) = 1.3\left\{\ln(1+r/0.19) - \arctan(r/0.19) + 0.5\ln\left[1+(r/0.19)^2\right]\right\} \quad (7)$$

for the Burkert fit. In the strong stripping scenario (see Sect. 2.4) we obtain instead

$$M^{\rm diff}_{\rm dark}/(10^{14}\,M_\odot) = 3.6\left[\ln(1+r/0.28) - r/0.28(1+r/0.28)^{-1}\right] \quad (8)$$

for the NFW fit, and

$$M^{\rm diff}_{\rm dark}/(10^{14}\,M_\odot) = 1.3\left\{\ln(1+r/0.19) - \arctan(r/0.19) + 0.5\ln\left[1+(r/0.19)^2\right]\right\} \quad (9)$$

for the Burkert fit.

Note that the best-fit NFW concentration values ($c = 7 \pm 1$ and $c = 10^{+4}_{-2}$, respectively, for the DM and DM diffuse profiles) are similar to the predictions of ΛCDM cosmological simulations (e.g. Dolag et al. 2004).

Our results are for clusters on average, and it is possible that individual clusters are characterized by different types of mass profiles (see, e.g., Ettori et al. 2002). Our results provide new constraints relative to most recent analyses (e.g. van der Marel et al. 2000; KBM) in that we derive the *dark*, rather than the *total* mass distribution. Łokas & Mamon (2003) did consider the *dark* matter distribution, but only of one cluster (Coma), while we have examined a sample of 59 clusters. Moreover, they did not subtract the contribution of subhaloes from the DM profile.

The major uncertainty in our analysis is due to the still rather limited number of available cluster galaxies with redshifts. Other sources of uncertainties (such as systematics in the knowledge of the IC gas density profile at large radii, or of the subhalo stripping efficiency), are smaller. With a larger data-set it will be possible to improve the constraints on the cluster mass profile, due to a better definition of the projected phase-space distribution of cluster members, and their orbital anisotropy. Improvements over the current analysis are therefore expected from the use of larger samples of clusters extracted from the Sloan Digital Sky Survey (e.g. Abazajian et al. 2004), which should allow a factor ∼3 increase in size with respect to the ENACS data-set used here (see Goto 2005).

Acknowledgements. We thank Gary Mamon for useful discussion. We also thank the anonymous referee for useful and constructive remarks. This research was partially supported by the Italian Ministry of Education, University, and Research (MIUR grant COFIN2001028932 "Clusters and groups of galaxies, the interplay of dark and baryonic matter").

References

Abazajian, L., Adelman-Mc Carthy, J. K., Agüeros, M. A., et al. 2004, AJ, 128, 502
Adami, C., Biviano, A., Durret, F., & Mazure, A. 2005, A&A, 443, 17
Allen, S. W., Ettori, S., & Fabian, A. C. 2000, MNRAS, 324, 877
Arieli, Y., & Rephaeli, Y. 2003, New A, 8, 517
Athreya, R. M., Mellier, Y., van Waerbeke, L., et al. 2002, A&A, 384, 743
Binney, J., & Tremaine, S. 1987, Galactic Dynamics (Princeton: Princeton University Press)
Biviano, A., & Girardi, M. 2003, ApJ, 585, 205
Biviano, A., & Katgert, P. 2004, A&A, 424, 779
Biviano, A., Girardi, M., Giuricin, G., Mardirossian, F., & Mezzetti, M. 1992, ApJ, 396, 35
Biviano, A., Katgert, P., Thomas, T., & Adami, C. 2002, A&A, 387, 8
Borriello, A., Salucci, P., & Danese, L. 2003, MNRAS, 341, 1109
Broadhurst, T., Takada, M., Umetsu, K., et al. 2005, ApJ, 619, L143
Burkert, A. 1995, ApJ, 447, L25
Carlberg, R. G., Yee, H. K. C., & Ellingson, E. 1997, ApJ, 476, L7
Cavaliere, A., & Fusco-Femiano, R. 1978, A&A, 70, 677
Dahle, H., Hannestad, S., & Sommer-Larsen, J. 2003, ApJ, 588, L73
de Blok, W. J. G., & Bosma, A. 2002, A&A, 385, 816
de Blok, W. J. G., Bosma, A., & McGaugh, S. 2003, MNRAS, 340, 657
Demarco, R., Magnard, F., Durret, F., & Márquez, I. 2003, A&A, 407, 437
Diemand, J., Moore, B., & Stadel, J. 2004, MNRAS, 353, 624
Dolag, K., Bartelmann, M., Perrotta, F., et al. 2004, A&A, 416, 853
Ettori, S. 2003, MNRAS, 344, L13
Ettori, S., De Grandi, S., & Molendi, S. 2002, A&A, 391, 841
Fukugita, M., Shimasaku, K., & Ichikawa, T. 1995, PASP, 107, 945
Gao, L., De Lucia, G., White, S. D. M., & Jenkins, A. 2004, MNRAS, 352, L1
Gavazzi, R., Mellier, Y., Fort, B., Cuillandre, J.-C., & Dantel-Fort, M. 2004, A&A, 422, 407
Gentile, G., Salucci, P., Klein, U., Vergani, D., & Kalberla, P. 2004, MNRAS, 351, 903
Gill, S. P. D., Knebe, A., Gibson, B. K., & Dopita, M. A. 2004, MNRAS, 351, 410
Girardi, M., Fadda, D., Giuricin, G., et al. 1996, ApJ, 457, 61
Gonzalez, A. H., Zabludoff, A. I., & Zaritsky, D. 2005, ApJ, 618, 195
Goto, T. 2005, MNRAS, 359, 1415
Jee, M. J., White, R. L., Benítez, N., et al. 2005, ApJ, 618, 46
Katgert, P., Mazure, A., Perea, J., et al. 1996, A&A, 310, 8
Katgert, P., Mazure, A., den Hartog, R., et al. 1998, A&AS, 129, 399
Katgert, P., Biviano, A., & Mazure, A. 2004, ApJ, 600, 657 (KBM)
Kelson, D. D., Zabludoff, A. I., Williams, K. A., et al. 2002, ApJ, 576, 720
Lin, Y.-T., & Mohr, J. J. 2004, ApJ, 617, 879
Łokas, E. L., & Mamon, G. A. 2003, MNRAS, 343, 401
Łokas, E. L., Wojtak, R., Gottlöber, S., Mamon, G. A., & Prada, F. 2006, MNRAS, in press
Mamon, G. A., & Boué, G. 2006, in preparation
Mohr, J. J., Mathiesen, B. J., & Evrard, A. E. 1999, ApJ, 517, 627
Moore, B., Quinn, T., Governato, F., Stadel, J., & Lake, G. 1999, MNRAS, 310, 1147
Murante, G., Arnaboldi, M., Gerhard, O., et al. 2004, ApJ, 607, L83
Natarajan, P., Loeb, A., Kneib, J.-P., & Smail, I. 2002, ApJ, 580, L17
Navarro, J. F., Frenk, C. S., & White, S. D. M. 1996, ApJ, 462, 536 (NFW)
Navarro, J. F., Hayashi, E., Power, C., et al. 2004, MNRAS, 349, 1039
Nelson, A. E., Gonzalez, A. H., Zaritsky, D., & Dalcanton, J. J. 2002, ApJ, 566, 103
Neumann, D. M. 2005, A&A, 439, 465
Nevalainen, J., Markevitch, M., & Forman, W. 2000, ApJ, 536, 73
Popesso, P., Biviano, A., Böhringer, H., Romaniello, M., & Voges, W. 2005, A&A, 433, 431
Pratt, G. W., & Arnaud, M. 2005, A&A, 429, 791
Reiprich, T. H., & Böhringer, H. 2002, ApJ, 567, 716
Ricotti, M. 2003, MNRAS, 344, 1237
Rines, K., & Diaferio, A. 2006 [arXiv:astro-ph/0602032]
Rines, K., Geller, M. J., Kurtz, M. J., & Diaferio, A. 2003, AJ, 126, 2152
Salucci, P., & Persic, M. 1999, MNRAS, 309, 923
Sanchis, T., Łokas, E. L., & Mamon, G. A. 2004, MNRAS, 347, 1198
Sand, D. J., Treu, T., Smith, G. P., & Ellis, R. S. 2004, ApJ, 604, 88
Shankar, F., Lapi, A., Salucci, P., De Zotti, G., & Danese, L. 2006, ApJ, accepted [arXiv:astro-ph/0601577]
Springel, V., White, S. D. M., Tormen, G., & Kauffmann, G. 2001, MNRAS, 328, 726
Takahashi, K., Sensui, T., Funato, Y., & Makino, J. 2002, PASJ, 54, 5
Thomas, T., & Katgert, P. 2006, A&A, 446, 19
van den Bosch, F. C., Tormen, G., & Giocoli, C. 2005, MNRAS, 359, 1029
van der Marel, R., Magorrian, J., Carlberg, R., Yee, H., & Ellingson, E. 2000, AJ, 119, 2038